Computers and Mathematics with Applications 61 (2011) 3577–3584

Contents lists available at ScienceDirect

Computers and Mathematics with Applications

journal homepage: www.elsevier.com/locate/camwa

# Lattice Boltzmann simulation of cavitating bubble growth with large density ratio

Xiao-Peng Chen [a,*], Cheng-Wen Zhong [b], Xu-Long Yuan [c]

[a] School of Mechanics, Civil Engineering and Architecture, Northwestern Polytechnical University, Xi'an, Shaanxi, 710072, PR China

[b] School of Aeronautics, Northwestern Polytechnical University, Xi'an, Shaanxi, 710072, PR China

[c] School of Marine Technology, Northwestern Polytechnical University, Xi'an, Shaanxi, 710072, PR China

ARTICLE INFO

*Article history:*
Received 27 October 2009
Received in revised form 9 July 2010
Accepted 13 July 2010

*Keywords:*
Cavitation
Phase transition
Bubble dynamics
Lattice Boltzmann method
Equation of state
High density ratio

ABSTRACT

Natural cavitation is defined as the formation of vapor bubbles in a flow due to the pressure falling below the liquid's vapor pressure. The inception of the cavitation bubble is influenced by a lot of aspects, such as impurities, turbulence, liquid thermal properties, etc. In this paper, the exact difference method (EDM) and the Carnahan–Starling real-gas equation of state (EOS) are coupled in the Shan–Chen multiphase lattice Boltzmann model, which is validated as being suitable for simulating high liquid/vapor density ratio multiphase flows. The 2D cavitation "bubble" growth is simulated under a quiescent and shear flow in the inception stage. Besides yielding the large density ratio, the real-gas EOS also leads to apparently different compressibilities for liquid and vapor. The results agree with Rayleigh–Plesset predictions much better than those of a previous publication [X. Chen, Simulation of 2D cavitation bubble growth under shear flow by lattice Boltzmann model, Communications in Computational Physics 7 (2010) 212–223]. In the meantime, a comparison is conducted for single-bubble behavior under different shear rates, with reduced temperature $T/T_{critical} = 0.6891$ and relaxation time $\tau = 1.0$. The simulation results show that the cavitation bubble deformation is consistent with the bubble dynamics, $D \propto \mathrm{Ca}$, where $D$ and Ca are the bubble deformation and the capillary number respectively. The shear rate hardly influences the bubble growth rate.



## 1. Introduction

Natural cavitation is defined as the phenomenon of the formation of vapor bubbles in a flow due to the pressure falling below the liquid's vapor pressure, which can cause degradation of fluid machinery performance [1,2] *and* drag reduction for high speed underwater vehicles [3]. In the past few decades, numerous efforts have contributed to the study of cavitation bubble inception [4,5], which can be treated as the initial condition for the bubble evolution. However, study shows that the cavitation inception is very complex. It is influenced by the number and qualities of the nuclei in the liquids, the flow structure, thermodynamic parameters, etc. Different inception forms were found, including the bubble band, bubble ring, traveling bubble, traveling patch, fixed patch, and developed attached cavitation [4].

In addition to the experimental and scaling analysis, numerical simulation is conducted widely as a powerful tool for cavitation study. Vortmann et al. [6] applied the volume of fluid method coupled with thermodynamic models to predict typical effects of cavitations. By the finite volume method, Chau et al. [7] studied the hydrodynamic characteristics of foils. Particular emphasis was placed by Kunz et al. [8] on solving two-phase Reynolds averaged Navier–Stokes equations

* Corresponding author.
*E-mail addresses:* xchen76@nwpu.edu.cn (X.-P. Chen), zhongcw@nwpu.edu.cn (C.-W. Zhong), yuanxulong@nwpu.edu.cn (X.-L. Yuan).

0898-1221/$ – see front matter © 2010 Elsevier Ltd. All rights reserved.
doi:10.1016/j.camwa.2010.07.018

(RANS), including the prediction strategy, flux evaluation, limiting strategies etc. Senocak and Shyy [9] applied a pressure–velocity–density coupling scheme to handle the large density ratio cavitating flow. In these classical partial differential equation based numerical simulations, two major obstacles must be overcome. The first one is establishing the numerical scheme. Because phase properties, such as density and viscosity, vary steeply across the interface, the numerical schemes should be designed carefully to prevent nonphysical oscillations. Limiting strategies, filtering techniques and/or sophisticated interface updating algorithms should be applied. Secondly, the phase transition model should be postulated correctly according to the thermodynamic fundamentals.

In recent decades, lattice Boltzmann methods (LBM) have emerged as attractive CFD methods, based on the mesoscale particle dynamics [10–12]. Some sophisticated flow phenomena, such as interfacial flow and reactive flow, are simulated successfully by the particle method, where the particle motion is simply divided into "collision" and "stream" loops. Shan and Chen [13] postulated a long range interaction, by which the liquid phase transition and interfacial tension were simulated perfectly. Swift et al. [14] coupled the Cahn–Hilliard free energy formula with the LBM. Phase separation and two-phase flow modeling were validated as being feasible. The key issue of the two models is reproducing the non-ideal gas EOS. So far, multiphase LBM have been applied in many fields [15,16], and large density ratio models attract great attention. For instance, Yuan and Schaefer [17] compared different EOSs applied in the Chen–Shan model. Excellent performance of Carnahan–Starling EOSs is proved in multiphase flow simulations with the density ratio over $10^3$. Kupershtokh et al. [18] recently improved the maximum ratio to be $10^7$ by coupling a proper EOS with the Zhang–Chen approach [19]. The model is also applied in dielectric liquid discharge simulations [20].

On the other hand, there are a few LBM simulations with a phase transition. Zhang and Chen [19] simulated the thermodynamic multiphase flow with the liquid–vapor density ratio of 3. In 2005, Sukop and Or [21] validated the capability of the LBM to simulate the cavitation problems using the Shan–Chen model. 2D bubble evolution (growth or collapse) was reported. Chen [22] simulated the cavitating bubble growth with the LBM in both quiescent and shear flows, where the results are compared with the Rayleigh–Plesset equation. However, in the latter work, the density ratio of the two phases was limited.

In this paper, the Carnahan–Starling real-gas EOS is applied to obtain a high density ratio liquid–vapor system. *The goal of this paper is to demonstrate the feasibility of using the LBM in qualitative cavitation simulations, which can be regarded as a starting point for future work.*

With this model, we also intend to study the 2D cavitation bubble growth under shear flow during its inception stage, which is often lacking in traditional numerical simulations. The scientific definition of the inception is adopted in our work, which means initial rapid growth of vapor-filled and gas-filled bubbles as a consequence of hydrodynamic forces [4]. In the situation of shear flow, the results are compared with the quiescent case in order to analyze the shear flow influences.

The rest of the paper is organized as follows. In Section 2, the Shan–Chen multiphase LBM method coupled with the Carnahan–Starling equation of state is introduced briefly. The exact difference method (EDM) is applied in the forcing term treatment. The flow domain setup is described in this section as well. In Section 3, the parameter setting and bubble growth under quiescent and shear flow are analyzed, and are compared with Rayleigh–Plesset and bubble dynamic models respectively. Conclusions are drawn in Section 4.

## 2. Mathematical models and the computational domain

### 2.1. Lattice Boltzmann model

A crucial idea of the lattice Boltzmann model is that both the location and velocity of the particles are discretized (see Fig. 1). The typical LB equation is presented as

$$f_i(\mathbf{x}+\mathbf{e}_i\Delta t, t+\Delta t) - f_i(\mathbf{x}, t) = -\frac{1}{\tau}\cdot(f_i(\mathbf{x}, t) - f_i^{\mathrm{eq}}(\mathbf{x}, t)) + \Delta f_i, \tag{1}$$

where $f_i$ ($i = 0, 1, \ldots, b$) denotes the particle velocity distribution function along the $i$th direction, $f_i^{\mathrm{eq}}$ the corresponding local equilibrium distribution satisfying the Maxwell distribution. $\mathbf{x}$, $\mathbf{e}_i$ are the lattice site coordinates and the particle velocities towards the nearest neighbor sites respectively. $b$ is the number of the neighbors. The lattice Boltzmann equation implies two kinds of particle operations, streaming and collision. On the left hand side of Eq. (1), particles jump from the local site, $\mathbf{x}$, to its nearest neighbor sites, $\mathbf{x}+\mathbf{e}_i\Delta t$, in each time step, $\Delta t \equiv 1$. On the right hand side, the collision leads to loss or gain of the particles with velocity of $\mathbf{e}_i$. After collision, the velocity distribution will relax to an equilibrium distribution, $f_i^{\mathrm{eq}}$. $\tau$ is the collision relaxation time. $\Delta f_i$ is the body force term which will be discussed in the Section 2.2.

In this study, the D2Q9 model is applied, which is depicted in Fig. 1. The equilibrium velocity distribution reads

$$f_i^{\mathrm{eq}}(x, t) = w_i\rho(x)\left[1 + 3\frac{\mathbf{e}_i\cdot u}{c^2} + \frac{9}{2}\frac{(\mathbf{e}_i\cdot u)^2}{c^4} - \frac{3}{2}\frac{u^2}{c^2}\right], \tag{2}$$

where the weights $w_i$ are 4/9 for the rest particles ($i = 0$), 1/9 for $i = 1, 2, 3, 4$, and 1/36 for $i = 5, 6, 7, 8$ (as in Fig. 1). $\mathbf{u}$, $\mathbf{c}$ are the macrovelocity and the lattice speed respectively. The corresponding macrovariables are defined as

$$\rho = \sum_{i=0}^{8} f_i \tag{3}$$

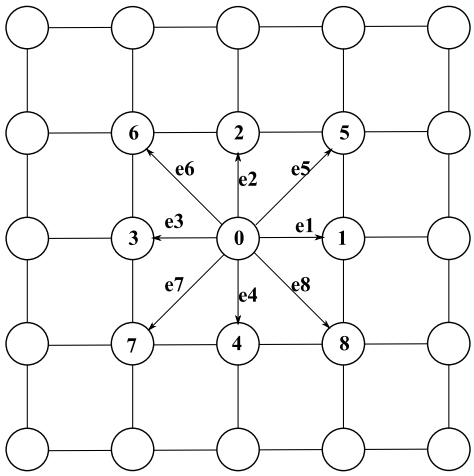


**Fig. 1.** Schematic diagram for the D2Q9 model.

$$\rho\mathbf{u} = \sum_{i=0}^{8}(f_i \cdot \mathbf{e}_i) \tag{4}$$

$$\nu = (2\tau - 1)/6 \tag{5}$$

where $\rho$, $p$ and $\nu$ denote density, pressure and kinematic viscosity, respectively. For the typical LBM, the ideal gas equation of state is valid, i.e. $p = \rho/3$.

### 2.2. The Shan–Chen model with the Carnahan–Starling EOS

According to Shan and Chen's multiphase model [13], long range interactions (or forces) between fluid particles result in non-ideal gas effects. The forces actually lead to phase separation, for both single and multiple components, if they are large enough. In our D2Q9 model, this is given by

$$\mathbf{F} = -\mathcal{G}\psi(\mathbf{x}, t)\sum_{i=1}^{8} w_i\psi(\mathbf{x} + \mathbf{e}_i\Delta t, t)\mathbf{e}_i, \tag{6}$$

where $\mathcal{G}$ is the interaction strength, with $\mathcal{G} < 0$ representing attractive forces, and $\psi$ the effective density. However, the improper force term treatment will lead to relaxation time dependency of the density pairs. The exact difference method (EDM) is proven to result in $\tau$-independent density pairs [18], where the force contribution in Eq. (1) is expressed as

$$\Delta f_i = f_i^{\mathrm{eq}}(\rho, \mathbf{u} + \Delta\mathbf{u}) - f_i^{\mathrm{eq}}(\rho, \mathbf{u}), \tag{7}$$

where $\Delta\mathbf{u} = \mathbf{F}\Delta t/\rho$. The simplified pressure is then obtained after correlating Eq. (1) with Navier–Stokes equations by Chapman–Enskog expansion [13]:

$$p = \rho c_s^2 + \frac{\mathcal{G}}{6}\left[\psi(\rho)^2\right], \tag{8}$$

which is a non-ideal gas EOS. According to the critical point condition (as pointed out later), a critical value of $\mathcal{G}_c$ can be obtained. For $\mathcal{G} < \mathcal{G}_c$, at a single pressure, two densities of the same material can coexist, namely, phase aggregation. The interfacial tension, which stems from inter-molecular forces, could be evaluated simply through the pressure difference across a circular interface.

Instead of giving $\psi$ directly, it can be calculated from several different existing EOSs according to Eq. (8) [17,23], namely,

$$\psi(\rho) = \sqrt{\frac{6(p - \rho c_s^2)}{\mathcal{G}}}. \tag{9}$$

The EOS could be the Carnahan–Starling real-gas EOS (C–S EOS),

$$\tilde{p} = c\tilde{\rho}\tilde{T}\frac{1 + b\tilde{\rho} + b\tilde{\rho}^2 - b\tilde{\rho}^3}{(1 - b\tilde{\rho})^3} - a\tilde{\rho}^2 \tag{10}$$

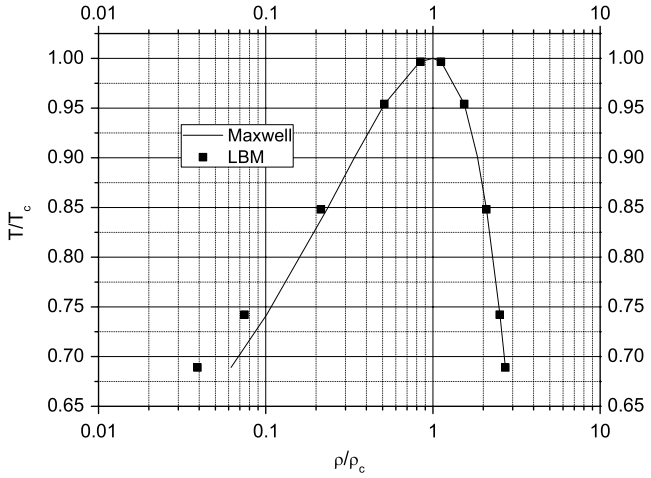


**Fig. 2.** Coexistence curves ($\tau = 1.0$). ■: LBM simulation (C–S EOS); curve: Maxwell equal-area rule prediction.

or others, such as vdW, R–K EOSs etc. Dimensionless variables are used in Eq. (10) ($\tilde{p} = \frac{p}{p_c}, \tilde{T} = \frac{T}{T_c}, \tilde{\rho} = \frac{\rho}{\rho_c}$, where $T_c, p_c, \rho_c$ are the corresponding values at the critical point). To satisfy the critical point conditions,

$$\tilde{p} = 1, \qquad \tilde{\rho} = 1, \qquad \tilde{T} = 1, \qquad \left(\frac{\partial \tilde{p}}{\partial \tilde{\rho}}\right)_{\tilde{T}} = 0, \qquad \left(\frac{\partial^2 \tilde{p}}{\partial \tilde{\rho}^2}\right)_{\tilde{T}} = 0$$

the parameters are calculated as

$$a = 3.852462257, \qquad b = 0.1304438842, \qquad c = 2.785855166.$$

It is demonstrated that a large density ratio could be obtained by using the Shan–Chen model with a proper EOS [17]. In this paper, we adopt Eq. (10), and the temperature $\tilde{T} = 0.5831, 0.6361, 0.6891$ respectively. With $\tau = 1.0$, a density ratio of 50–200 is captured successfully. It is worthy of noting that $\mathcal{G}$ becomes unimportant in this case; for this, the only requirement is to ensure that the whole term inside the square root of Eq. (9) is positive.

To check the feasibility of the model, the binodal curve is first plotted as in Fig. 2, where the curve is predicted by the Maxwell equal-area rule. LBM simulation is qualitatively good for the prediction, especially for the liquid density. The basic assumptions for the Rayleigh–Plesset equation include negligibly low density of vapor and that the bubble pressure (saturated vapor pressure) only depends on the temperature. In this work, the EOS only plays roles during the bubble growth indirectly through the interfacial tension. Therefore, the errors for EOS are tolerable.

### *2.3. The computational domain*

In this work, the computational domains, $3500 \times 3500$ and $500 \times 400$ ($\delta x = \delta y \equiv 1$), are set for bubble growth simulation in quiescent and shear flow, respectively (as shown in Fig. 3). The former is large enough to suppress the boundary reflected waves, and the latter is only used to produce a large enough shear rate under the low Mach number assumption. In both domains, the upper and lower boundaries are imposed on constant velocities, which have the same values but opposite directions ($v_B = 0$ and $\pm 0.02, \pm 0.05, \pm 0.08, \pm 0.1$ respectively). The Zou–He boundary condition model [24] is applied on these two sides. The constant density/pressure is imposed on the left and right boundaries. The value of the boundary density is set following Sukop's procedure [25]. For a certain fluid, the equilibrium phase densities ($\rho_L$ and $\rho_v$ for liquid and vapor respectively) are computed in the flat-interface liquid–vapor system with the periodic boundary condition first (the subscripts $L$ and $v$ denote liquid and vapor in the rest of the paper). The density boundary condition ($\rho_{\text{Bound}}$) is then set with values lower than $\rho_L$ by 0.5% (lower than the critical pressure for cavitation).

With proper parameters, the bubble will collapse if the initial size is smaller than $R_{\text{crt}} = 4$ due to the large interfacial tension. To catch the influence of the shear flow on the bubble growth, $R_{\text{initial}} > 5$ is chosen. The initial density distribution in the domain is set to $\rho_B = \rho_v$ inside the bubble and $\rho_{\text{out}} = \rho_{\text{Bound}} = \rho_L \cdot 99.5\%$ outside the bubble. The velocity is initialized with a fully developed shear flow profile (as in Fig. 3), and the velocity distribution function, $f_i$, is calculated through Eq. (2).

## 3. Results and discussion

The major purpose of this paper is to study the cavitating bubble growth in both quiescent and shear flows for high density ratio liquid–vapor pairs. To obtain the proper initial and boundary conditions and the liquid properties, a computational domain of $1000 \times 1000$ ($\delta x = \delta y \equiv 1$) with periodic boundary conditions is adopted, which is believed to result in the

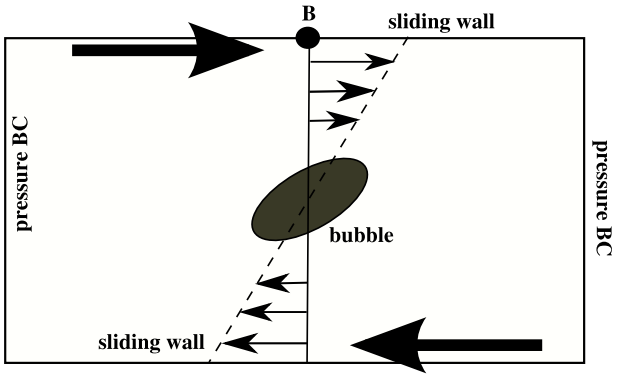


**Fig. 3.** Computational domain.

same results as the larger domain. The equilibrium density is obtained for a flat-interface liquid–vapor system, while the interfacial tension, $\sigma = (p_{\text{in}} - p_{\text{out}}) \cdot R_{\text{bubble}}$, is obtained for circular ones, where $p_{\text{in}}$, $p_{\text{out}}$ and $R_{\text{bubble}}$ are pressures inside and outside the bubble and the bubble radius, respectively.

According to the results, $\tau = 1.0$ is chosen in all cases. Three temperatures, $\tilde{T} = 0.5831$, 0.6361 and 0.6891, are tested for quiescent cases, to give a full validation of the feasibility of the method. For the shear flows, $\tilde{T} = 0.6891$ is chosen and the corresponding density ratio ($\tilde{\rho_v} = 0.040$, $\tilde{\rho_L} = 2.706$) is large enough to satisfy the assumption of the Rayleigh–Plesset equation.

### 3.1. Bubble growth in quiescent liquid

It is well known that Rayleigh–Plesset equation predicts spherical bubble growth precisely. Chen [22] calculated the Rayleigh–Plesset equation under the condition of 2D, which is proved to be boundary condition sensitive:

$$\ln\left(\frac{r_\infty}{R}\right) \cdot \left(\dot{R}^2 + R\ddot{R}\right) - \frac{\dot{R}^2}{2} - \frac{2\mu_L}{\rho_L R}\dot{R} + \frac{\sigma}{\rho_L R} = \frac{p_B - p_\infty}{\rho_L} \tag{11}$$

where $R$ is the bubble radius, $r_\infty$ the far field boundary location, $\mu_L$ the liquid's viscosity, $p_B$ and $p_\infty$ the pressures in the bubble and at infinity respectively. One of the major assumptions of the Rayleigh–Plesset equation is that the liquid density is greatly larger than the vapor density [1]; therefore, it is supposed that the low liquid–vapor density ratio leads to several kinds of simulation errors, as in Chen's work [22].

In Fig. 4, the simulated results are plotted with $\tilde{T} = 0.5831, 0.6361, 0.6891$ (with corresponding initial density ratios 200, 77, 50 roughly). During the whole process, they agree quite well with the theoretical predictions from Eq. (11), which are obtained by the Runge–Kutta method. Here, the exact values of the parameters, like $\rho_L$, $\sigma$, $\mu_L$, $p_\infty$, $p_B$ (the measured value is lower than $p(\rho_v)$ by 2%), measured from the simulations, are applied in the equation (the equation should be true for any fundamental units). As in the simulation, $r_\infty = 1750$ is applied to Eq. (11). The initial conditions for the prediction, $R_0$ and $\dot{R}_0$, are measured through the LB simulations at time $= 180$ to eliminate the errors caused by the initial density relaxation procedure.

As in Eq. (11), the bubble growth is mainly driven by the pressure difference between the inside and outside of the bubble, and the mass transition influence can be neglected under the condition of large density ratio. Therefore, the EOS only influences the procedure through the interfacial tension theoretically (the liquid density is predefined according to the boundary condition).

### 3.2. Bubble growth in shear flow

The nonspherical cavitation bubble inception plays important roles in wake cavitation, where high shear rate flow couples with vortex evolution. Moreover, bubble deformation in a second immiscible liquid is full of scientific and technical values [26]. In this section, we focus on the bubble growth in pure shear flow. To produce large enough shear rates, the domain is set as $400 \times 500$ in this section and the initial bubble size as 5. Although it will cause some errors, such as boundary reflected pressure waves, the shear rate effects can be highlighted here. And the cavitation bubble has undergone shear flow with the shear rate $G_s = \frac{v_B}{h}$, where $h$ is the gap size between the upper and lower walls. In this section, $\tilde{T} = 0.6891$, $\tau = 1.0$ and the density ratio $\frac{\rho_L}{\rho_v} = 46$.

A typical bubble growth sequence is shown in Fig. 5.

For the procedures, two parameters may be worth comparing: the deformation and the growth rate. Following Rallison [26], it is usual to define a dimensionless deformation $D$ by

$$D = (l - b)/(l + b) \tag{12}$$

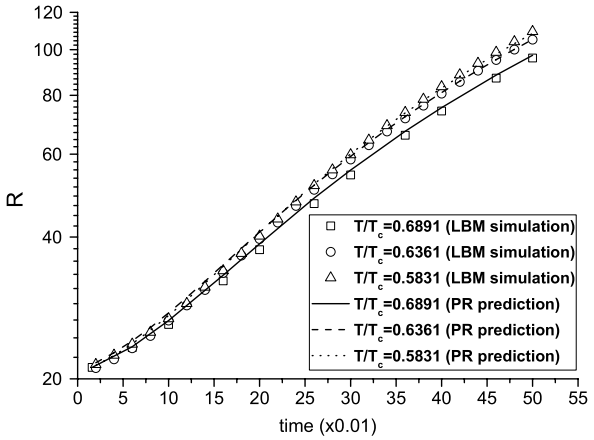


**Fig. 4.** Bubble growth in quiescent liquid. Comparison of the lattice Boltzmann simulation (LB simulated) and Rayleigh–Plesset equation predictions (RP prediction). The initial conditions for RP predictions are measured through the computed results, where: $\tilde{T} = 0.5831$: $R_{t=180} = 21.36$, $\dot{R}_{t=180} = 0.0047$; $\tilde{T} = 0.6361$: $R_{t=180} = 21.55$, $\dot{R}_{t=180} = 0.0046$; $\tilde{T} = 0.6891$: $R_{t=180} = 21.15$, $\dot{R}_{t=180} = 0.0038$.

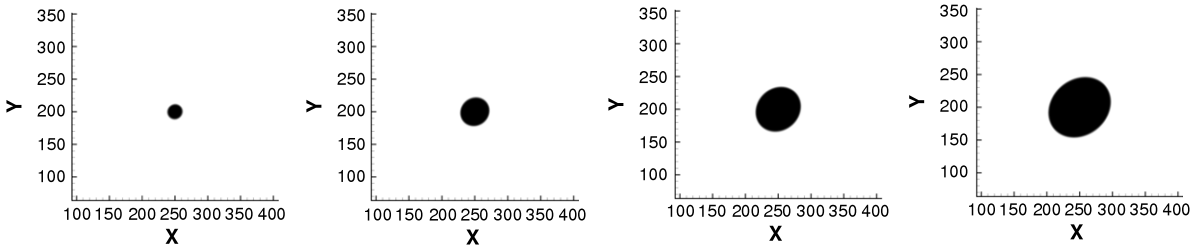


**Fig. 5.** Snapshots of bubble deformation in shear flow. $G_s = 5 \times 10^{-4}$. The interval between frames is 200 steps.

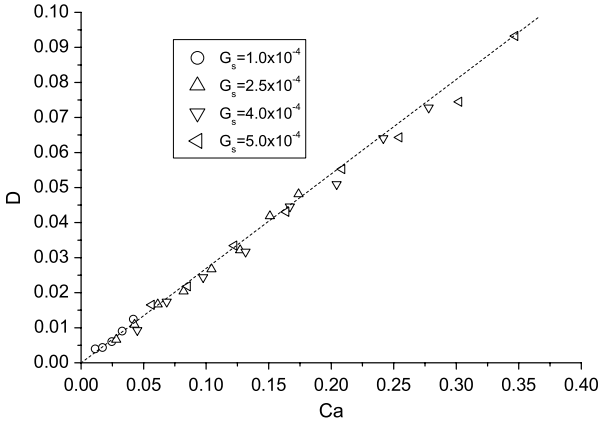


**Fig. 6.** The relationship between deformation, $D$, and capillary number, Ca. The simulation results are fitted by a linear relationship (dashed line).

where $l$ and $b$ are the largest and smallest distances from the bubble center to the interface, respectively. The deformations for all shear rates and time instants are plotted in the Fig. 6. Here, the vapor and liquid interface is defined at $\tilde{\rho} = 1.338$, which equals $\frac{\tilde{\rho}_v + \tilde{\rho}_L}{2}$ when $t = 100$.

In the Fig. 6, $\mathrm{Ca} = \mu_L G_s a/\sigma$ is the capillary number, which denotes the ratio of the shear force to the interfacial tension. The length scale $a$ is set as $0.5 \cdot (l + b)$. The linear relationship between Ca and $D$ implies that, in the inception stage, the viscous and interfacial tension effects dominate over the bubble deformation, which is typical for small scale flow [26]. Compared to using the original Shan–Chen model [22], in applying this method, the densities *relax* fast at the beginning stage of inception, and the fitting line of the points passes through the coordinate origin (dashed line in Fig. 6).

Comparing to setting $\psi$ directly and the lower density ratio cases [22], Fig. 7 shows much smaller differences among the bubble growth speeds with various shear rates. Chen's work showed roughly 1.0% of bubble volume discrepancy at time $= 800$, while Fig. 7 shows about 0.3%, where the bubble volume is defined as the area in the domain with density

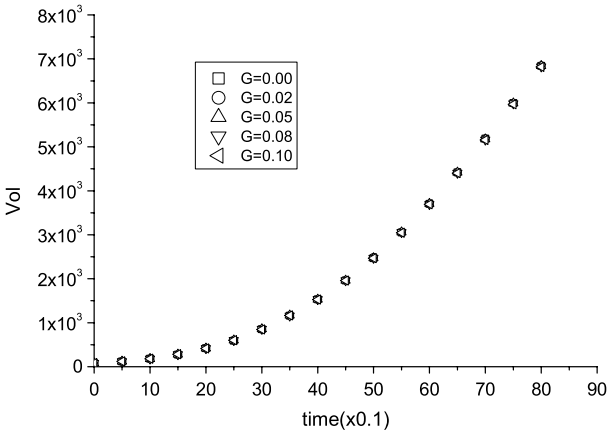


**Fig. 7.** Bubble growth in shear flow.

smaller than $\frac{1}{2} \cdot (\tilde{\rho}_v + \tilde{\rho}_L)$. The small influence of deformation (or shear flow) on the bubble growth stems from the fact that the cavitating bubble growth is driven by the pressure difference [1].

## 4. Conclusions

In this paper, we simulate the cavitating bubble growth in rest and shear flows with the Shan–Chen single-component multiple-phase lattice Boltzmann model. The C–S equation of state is applied to obtain the proper density ratio and compressibility for liquid and vapor. The EDM is utilized to treat the force term, which results in a more precise binodal curve. The feasibility of the model is validated. The conclusions can be drawn as follows:

- By applying the C–S EOS with proper constants, the real-gas effects can be achieved. The contribution is twofold. Both the high density ratio for the liquid–vapor pair and the liquid–vapor compressibility difference lead to a more precise prediction for cavitating bubble growth in a quiescent environment.
- In shear flow, the bubble will be stretched and the deformation $D \propto \mathrm{Ca}$, which is consistent with normal bubble dynamics. Although the shear rate, or Ca, could lead to different bubble deformation, it hardly influences the bubble growth rate according to the simulations.
- The 2D cavitating bubble growth is boundary condition sensitive, which is proved from both the Rayleigh–Plesset equation and LBM predictions.

## Acknowledgements

Support from the NSF of China (Grant No. 10902087), University Foundation for Fundamental Research of NPU, Research Fund for the Doctoral Program of Higher Education of China and Chinese New Century Excellent Talents Program in University (NCET-07-0688) is gratefully acknowledged. And the author is also grateful to the reviewers of this paper for valuable and inspiring comments.

## References

[1] C. Brennen, Cavitation and Bubble Dynamics, Oxford University Press, New York, 1995.
[2] R. Arndt, Cavitation in fluid machinery and hydraulic structures, Annu. Rev. Fluid Mech. 13 (1981) 273–328.
[3] C. Lu, Y. He, X. Chen, et al., Numerical and experimental research on cavitating flows, in: F. Zhuang, C. Lu (Eds.), New Trends in Fluid Mechanics Research, 5th International Conference on Fluid Mechanics, Tsinghua Univ. Press, Shanghai, China, 2007, pp. 45–52.
[4] E. Rood, Review—mechanics of cavitation inception, J. Fluids Eng. 113 (1991) 163–175.
[5] R. Arndt, Cavitation vortical flows, Annu. Rev. Fluid Mech. 34 (2002) 143–175.
[6] C. Vortmann, G. Schnerr, S. Seelecke, Thermodynamic modeling and simulation of cavitating nozzle flow, Int. J. Heat Fluid Flow 24 (2003) 774–783.
[7] S. Chau, K. Hsu, J. Kouh, et al., Investigation of cavitation inception characteristics of hydrofoil sections via a viscous approach, Mater. Sci. Technol. 8 (2004) 147–158.
[8] R. Kunz, D. Boger, D. Stinebring, et al., A preconditioned Navier–Stokes method for two-phase flows with application to cavitation prediction, Comput. Fluids 29 (2000) 849–875.
[9] I. Senocak, W. Shyy, A pressure-based method for turbulent cavitating flow computations, J. Comput. Phys. 176 (2002) 363–383.
[10] S. Succi, The Lattice Boltzmann Equation for Fluid Dynamics and Beyond, Oxford Univ. Press, New York, 2001.
[11] D. Wolf-Gladrow, Lattice-Gas Cellular Automata and Lattice Boltzmann Models, Springer-Verlag, Berlin, 2000.
[12] S. Chen, G. Doolen, Lattice Boltzmann method for fluid flows, Annu. Rev. Fluid Mech. 30 (1998) 329–364.
[13] X. Shan, H. Chen, Lattice Boltzmann model for simulating flows with multiple phases and components, Phys. Rev. E 47 (1993) 1815–1819.
[14] M. Swift, W. Osborn, J. Yeomans, Lattice Boltzmann simulation of nonideal fluids, Phys. Rev. E 75 (1995) 830–834.
[15] W. Huang, Y. Li, Q. Liu, Application of the lattice Boltzmann method to electrohydrodynamics: deformation and instability of liquid drops in electrostatic fields, Chinese Sci. Bull. 52 (2007) 3319–3324.

[16] A. Tentner, H. Chen, R. Zhang, Simulation of two-phase flow and heat transfer phenomena in a boiling water reactor using the lattice Boltzmann method, Physica A 362 (2006) 98–104.
[17] P. Yuan, L. Schaefer, Equations of state in lattice Boltzmann model, Phys. Fluids 18 (2006) 042101.
[18] A. Kupershtokh, D. Medvedev, D. Karpov, On equations of state in a lattice Boltzmann method, Comput. Math. Appl. 58 (2009) 965–974.
[19] R. Zhang, H. Chen, Lattice Boltzmann method for simulations of liquid–vapor thermal flows, Phys. Rev. E 67 (2003) 066711.
[20] A.L. Kupershtokh, D.I. Karpov, D.A. Medvedev, et al., Stochastic models of partial discharge activity in solid and liquid dielectrics, IET Proc.: Sci. Meas. Technol. 1 (6) (2007) 303–311.
[21] M. Sukop, D. Or, Lattice Boltzmann method for homogeneous and heterogeneous cavitation, Phys. Rev. E 71 (2005) 046703.
[22] X. Chen, Simulation of 2D cavitation bubble growth under shear flow by lattice Boltzmann model, Commun. Comput. Phys. 7 (2010) 212–223.
[23] X. He, G. Doolen, Thermodynamic foundation of kinetic theory and lattice Boltzmann models for multiphase flows, J. Stat. Phys. 107 (1–2) (2002) 309–328.
[24] Q. Zou, X. He, On pressure and velocity boundary conditions for the lattice Boltzmann BGK model, Phys. Fluids 9 (1997) 1591–1598.
[25] M. Sukop, D. Thorne Jr., Lattice Boltzmann Modeling, Springer-Verlag, Berlin, Heidelberg, 2007.
[26] J. Rallison, The deformation of small viscous drops and bubbles in shear flows, Annu. Rev. Fluid Mech. 16 (1984) 45–66.